Hydrol. Earth Syst. Sci. Discuss., 9, 13693–13728, 2012
www.hydrol-earth-syst-sci-discuss.net/9/13693/2012/
doi:10.5194/hessd-9-13693-2012
© Author(s) 2012. CC Attribution 3.0 License.

Hydrology and Earth System Sciences Discussions

This discussion paper is/has been under review for the journal Hydrology and Earth System Sciences (HESS). Please refer to the corresponding final paper in HESS if available.

A probability of snow approach to removing cloud cover from MODIS Snow Cover Area products

V. López-Burgos[1,*], **H. V. Gupta**[1], **and M. Clark**[2]

[1]Hydrology and Water Resources, The University of Arizona, Tucson, AZ, USA
[2]Hydrometeorological Applications Program, Research Applications Laboratory, Boulder, CO, USA
[*]now at: USDA Forest Service, Rocky Mountain Research Station, Boise, ID, USA

Received: 17 October 2012 – Accepted: 14 November 2012 – Published: 13 December 2012

Correspondence to: H. V. Gupta (hoshin.gupta@hwr.arizona.edu)

Published by Copernicus Publications on behalf of the European Geosciences Union.

Abstract

Satellite remote sensing can be used to investigate spatially distributed hydrological states and fluxes for use in modeling, assessment and management. However, in the visual wavelengths, cloud cover can often obscure significant portions of the images. This study develops a rule-based, multi-step method for removing clouds from MODIS Snow Cover Area (SCA) images. The methods used include a combining images from more than one satellite, time interpolation, spatial interpolation, and estimation of the probability of snow occurrence based on topographic information. Applied over the Upper Salt River Basin in Arizona, the method reduced the degree of cloud obscuration by 93.8 % while maintaining a similar degree of image accuracy to that of the original images.

1 Introduction

Water in the Southwestern United States (SWUS) is a scarce resource, requiring efficient management to meet the growing demands of a rapidly growing population. Since approximately 1999, the Colorado River Basin has been experiencing a severe drought (Olster, 2005; Piechota et al., 2004). Several studies suggest that the drought could continue for an extended period of time (Gedalof and Smith, 2001; Hereford et al., 2002), and may even get worse.

In Arizona, the temporal distribution of annual precipitation is highly seasonal, having two distinctive peaks (Sheppard et al., 2002). Winter precipitation is particularly important because cooler temperatures allow the accumulation and persistence of snowpack at higher elevations (Jacobs et al., 2005), with spring snowmelt providing inflow to the reservoirs used for water supply and hydropower generation. In fact, even though only 39 % of winter precipitation in the Salt and Verde watersheds falls as snow (Serreze, 1999), snowmelt accounts for up to 85 % of the surface water supply for the Phoenix Metropolitan Area (Hawkins, 2006). Overall, snowmelt has been estimated to account

HESSD
9, 13693–13728, 2012

for ∼ 75 % of annual stream discharge in Western United States (Cayan, 1996). Similarly, even though only 25–50 % of average annual precipitation falls as snow, snowmelt has been shown to provide 40–70 % of groundwater recharge at several study sites in the SWUS (Earman et al., 2006). This is significant, because ∼ 40 % of Arizona's water supply is taken from the underlying aquifers (Megdal, 2004). However, with temperatures in the SWUS projected to rise by 1 °C or more over the next hundred years, the extent and persistence of snowpack is threatened. The ability to estimate and monitor the evolution of snowpack is therefore extremely important.

One way to generate spatially distributed estimates of snowpack is by interpolating point scale field measurements of "snow water equivalent" from SNOw TELemetry (SNOTEL) sites located across a watershed (e.g. Fassnacht et al., 2003). However, NASA MODIS remotely sensed data products are now routinely made available by the center for land remote sensing for global change research (Justice et al., 1998).

In this paper, we focus on the MOD10A1 and MYD10A1 Snow Cover Area (SCA) products derived from spectral imagery collected by the MODIS sensor aboard two satellite platforms (Terra and Aqua, respectively). These satellite platforms follow the same orbit within three hours of each other (therefore providing two observations of SCA per day), and have a higher spatio-temporal resolution (500 m, 1 day) than other available products such as AVHRR, NOAA, and Landsat. However, the accuracy of the MODIS SCA product is affected by several factors, including land cover type, snow depth conditions and the presence of cloud cover, even though the classification algorithm uses a "cloud mask" to reduce this problem (Justice et al., 1998; Hall and Riggs, 2007; Zhou et al., 2005; Klein and Barnett, 2003; Bitner et al., 2002; Simic et al., 2004; Tekeli et al., 2005).

Several techniques developed for reducing the cloud cover noise in SCA images have been reported in the literature (see Sect. 2). In this work, we investigate the performance of several such techniques over the Salt River Basin in Arizona, and develop a hybrid rule-based, multi-step method that computes the probability that a cloudy pixel is underlain by snow. Section 2 reviews the literature regarding snow cover imagery and

HESSD
9, 13693–13728, 2012

cloud obscuration, Sect. 3 describes the study region and data used, Sect. 4 discusses three existing and one new method for cloud removal from snow cover images, Sect. 5 reports the results of testing these methods over the Salt River watershed in Arizona, and Sect. 6 evaluates the results using ground truth data. Finally, in Sect. 7 we discuss the results and make suggestions for future work.

2 Review of the literature

2.1 Sensors providing Snow Cover Area imagery

Snow cover maps have been produced since 1966, using remotely sensed data gathered by polar orbiting NOAA satellites. The most widely used satellites/sensors have been the landsat thematic mapper (TM) and enhanced thematic mapper (ETM+), the NOAA-Advanced Very High Resolution Radiometer (AVHRR), the Geostationary Orbiting Earth Satellite (GOES), and the Terra and Aqua MODIS sensors.

The landsat-based thematic mapper was originally thought to provide the best data for snow cover mapping due to its high spatial resolution of 30 m. First launched in July 1982, that sensor has been decommissioned but the improved enhanced thematic mapper (launched in 1999) is currently operational and provides improved resolution in the thermal-infrared band (Caves et al., 1999). The sensor provides images with a swath width of 185 km and a repeat coverage interval of 16 days. Although providing superior spatial resolution, the limited temporal resolution limits its applicability for long-term snow cover mapping and modeling studies (Rango, 1985), making it unsuitable for studies in the SWUS where the snow cover is sparse and ephemeral, and where the snow can melt away in less than 16. Nonetheless, it has been used to evaluate MODIS snow cover products at river-basin scale areas (Justice et al., 1998), and as ground truth in accuracy studies of MODIS in conjunction with ground measurements (Hall and Riggs, 2007).

HESSD
9, 13693–13728, 2012

The Advanced Very High Resolution Radiometer (AVHRR) sensor, first launched in 1979 aboard the NOAA polar orbiting satellite, provides snow products (Carroll et al., 2001) with higher temporal frequency for the continental US and Canada. The sensor provides images with a swath width of 2399 km and a revisit time of 12 h (one daytime and one night time pass). While its lower spatial resolution (1 km) makes it difficult to use for snow mapping on small basins (Schmugge et al., 2002), studies on a 572.9 km^2 basin in the Pyrenees mountains of Spain found that the correlation between AVHRR and MODIS snow maps to be on the order of 0.8–0.9, even in smaller sub-basins with areas of $\sim 8.3\,km^2$. However, similar comparisons in the Columbia and Missouri River basins showed that, on average, MODIS SCA images classified fewer pixels as cloud than NOHRSC, indicating it to be a better resource for snow mapping in forested watersheds (Maurer et al., 2003).

The Moderate Resolution Imaging Spectroradiometer (MODIS) sensor, launched in 1999 and 2002 onboard the Terra and Aqua Earth Observing System satellites respectively, is designed to complement the Landsat-7 satellite in observing and monitoring Earth system changes (Justice et al., 1998). Daily, and 8-day composite, snow products (Hall and Riggs, 2007) are available globally at no cost and in a variety of resolutions and projections via the National Snow and Ice Data Center webpage (http://nsidc.org/data/modis/index.html). Due to its high spectral and spatial resolution it has become popular as an alternative to AVHRR-based snow maps. However, the accuracy of MODIS snow maps has been found to vary with land cover type (Justice et al., 1998). The most frequent errors are caused by difficulties in discriminating between snow and cloud and in the mapping of very thin snow. Nevertheless, despite propagation of errors from the daily products, errors of commission (mapping pixels as snow where there is no snow) have been found to be very low in the 8-day composite products (Hall and Riggs, 2007).

In general, studies have found the accuracy of MODIS snow products to be persistently good. Zhou et al. (2005) conducted an evaluation of MODIS SCA products over the Upper Rio Grande Basin and reported statistically significant correlations when

HESSD
9, 13693–13728, 2012

assessed against streamflow and SNOTEL measurements. However, clouds obscuration was reported to be a major cause of reduced accuracy. Another study, comparing MODIS snow-cover products with NOHRSC maps, found that "comparisons . . . over the snow season show good overall agreement with accuracies of 94 % and 76 % for MODIS and NOHRSC, respectively" (Klein and Barnett, 2003). As noted later by Hall and Riggs (2007), this study found that MODIS fails to map snow at depths less than 4 cm. Other validation studies have reported similar results (e.g. Bitner et al., 2002; Simic et al., 2004; Tekeli et al., 2005).

2.2 The problem of cloud obscuration

Overall, MODIS SCA products have been found to be useful for reducing uncertainty in knowledge of the extent and amount of snow. However, cloud cover has been found to significantly impact the usefulness of this data, and to cause problems for assimilation into hydrological models. For example, Mcguire et al. (2005) and Andreadis and Lettenmaier (2006) reported only being able to use SCA images for days where cloud obscuration was less than 20 % of the grid cell, while Rodell and Houser (2004) used 6 % as the threshold for minimum visibility. Consequently, several investigations into techniques for removing cloud cover from SCA images have been reported.

Of course, the cloud obscuration problem is not intrinsic to MODIS SCA products, due to the fact that sensors for the visible portion of the electromagnetic spectrum cannot see through clouds, and due to the similarities in the spectral signatures of snow and clouds. The visible and thermal bands can be used to discriminate between snow and clouds (see reviews by Lucas and Harrison, 1990; Klein et al., 1998, 2000; Rigs and Hall 2002; Schmugge et al., 2002; etc.) and passive microwave can be used to infer snow extent, depth, water equivalent and state (Schmugge et al., 2002).

Various studies have attempted to reduce the degree of cloud obscuration in SCA image products. Lichtenegger et al. (1981) and Seidel et al. (1983) used elevation, slope, exposure, and brightness information from a Digital Terrain Model (DTM) to extrapolate snow cover from cloud-free to cloud-covered areas in digital landsat multispectral

HESSD
9, 13693–13728, 2012

scanner data, assuming that for each elevation zone the regions with equivalent exposure and slope angle carry the same amount of snow. Molotch et al. (2004) filtered NOHRSC SCA maps (based on AVHRR/GOES data) using gridded positive accumulated degree-days (ADD) and AVHRR derived binary SCA to obtain a threshold for defining snow cover in the Salt and Verde Rivers in Arizona. They reported temperature data to be helpful for estimating snow extent beneath clouds, and to thereby improve spatial and temporal continuity of SCA and SWE products.

Parajka and Blösch (2006) reported that although MODIS SCA had an average accuracy of 95 % when compared against snow data at 754 climate stations in Austria, clouds covered fully 63 % of the region (even worse in winter when interest in the snow product is higher). They tested a technique for cloud removal that combined MODIS Terra and Aqua data, used majority classification from the eight nearest pixels, and applied a one to seven day temporal window. The approach was found to be remarkably effective at cloud reduction, although accuracy was found to decrease in an almost linear fashion with the application of each filtering technique. Gafurov and Bárdossy (2009) applied the same techniques (with modifications) plus three additional filters – snow transition elevation, spatial combination of four neighboring pixels, and a time series of each pixel over an entire year – to the Kokcha Basin in Afghanistan. In a synthetic data evaluation they achieved complete removal of cloud cover and an overall accuracy of 91.49 %.

3 Study region and data used

The MODIS Terra sensor provides SCA map products having the best spatio-temporal resolution and accuracy. However, cloud obscuration reduces the value of these images and complicates the images use for data assimilation into models. In this study, we develop and test a method for cloud removal from MODIS SCA images over the Salt River Basin in Central Arizona.

HESSD
9, 13693–13728, 2012

3.1 Study area

The Upper Salt Basin (Fig. 1), having a drainage area of ~ 11 152.5 km^2, is a major source of surface water for the Phoenix Metropolitan Area. On an average annual basis, the precipitation varies from 15 to 47 inches, runoff is ~ 880 cfs, minimum temperature varies from 7 to 39 °F, and maximum temperature varies from 63 to 103 °F (PRISM CGOSU, 2006a, b). The elevation ranges between 674 m and 3472 m a.s.l., and land cover types are primarily ponderosa pine (65 %), chaparral (26 %), pinyon pine-juniper (10 %), and desert grassland (Rinne, 1975). Winter precipitation is of paramount importance, since snowmelt can account for up to 85 % of the usable water (Hawkins, 2006), and so snow accumulation and ablation are very important to water resources management.

The local water and power utility, the Salt River Project (SRP), currently relies on sporadic helicopter flights to verify snow cover extent. In addition, daily snowpack data from four SNOTEL locations at higher elevations in the eastern part of the watershed (where snow water storage is greatest; Fig. 1) are used for making streamflow forecasts, but this can lead to erroneous underestimates of streamflow since the point measurements are not representative of the areal pattern of snow accumulation. Consequently, the utility is interested in using remotely sensed SCA imagery to improve the accuracy of their forecasts.

3.2 MODIS Data

The MODIS SCA products used in this research (MOD10A1 and MYD10A1) are snow cover maps, created from spectral images obtained by the Terra and Aqua satellites. To generate these maps, NASA applies several algorithms based on the Normalized Difference Snow and Normalized Difference Vegetation indices (NDSI and NDVI respectively), as well as a cloud mask to distinguish snow and cloud pixels (Hall and Riggs, 2007). The cloud mask algorithm uses 14 of the 36 MODIS bands in 18 cloud spectral tests that start with an initial guess of whether snow or cloud is being viewed

HESSD
9, 13693–13728, 2012

so that appropriate processing paths and tests can be applied based on surface type, geographic location and ancillary data. The result – "cloudy", "clear" or "probably clear" – is reported for each pixel (Ackerman et al., 1998).

The products are provided on a Sinusoidal Grid Projection divided into 10° × 10° tiles (approximately 1200 × 1200 km at the equator) (Wolfeet al., 1998). The "h08v05" tile includes Arizona, Utah, Southern California, and parts of Northern Mexico. The data are provided in Hierarchical Data Format (HDF), as binary SCA, fractional SCA (FSCA) and snow albedo for each day, through the National Snow and Ice Data Center (NSIDC) webpage (http://nsidc.org/data/modis/index.html).

We used SCA data from 1 October 2004 to 31 May 2005 (8 months). ArcGIS9 ArcMap Version 9.3 was used to compute projection changes and for processing geographic information system data (e.g. digital elevation model). All image-processing computations were carried out using MATLAB 7.5.0.

Because the eventual goal is to assimilate the SCA images into a distributed hydrological model, a quick test was run in which the SCA data was upscaled from its native resolution of ∼ 500 m (51 375 pixels) to grids of ∼ 12.5 km (116 grids). However, the upscaled data exhibited irregular behavior, with many grids going from 100 % FSCA to 0 % FSCA from one day to the next, not properly reflecting the gradual onset of snowmelt. Figure 2 shows the FSCA time series for one grid overlayed upon a Snow Water Equivalent (SWE) time series for a SNOTEL station located inside the grid, and illustrates the large extent to which clouds cover the watershed during the study period. Figure 3a shows a pixel map of number of "days of snow" across the basin between 1 October and 31 May, constructed from the raw SCA data, clearly indicating that snow is being accumulated in the right places (higher elevations on the eastern side). To complement this, Fig. 3b shows a pixel map of number of days with clouds over the same period; note that this number ranges from 70–120 days (29–49 %) of the total 243 days in the study period. Overall, clouds cover 39 % of the SCA image pixels, mostly during periods of active snowfall. Further, it can sometimes be several days before the cloud

HESSD
9, 13693–13728, 2012

cover clears away, during which time some of the snow at lower elevations can melt away and therefore not be accounted for.

To simplify our analysis, the MODIS SCA images were first pre-processed to classify each pixel as belonging to only one of the following five categories – cloud (new code 1/original codes 11 and 50), error (new code 2/original codes 0, 254 and 255), snow (new code 3/original code 200), land (new code 4/original codes 25, 37, 39 and 100), and no decision (new code 5/original code 1). In addition, three new categories were added – missing day (new code 6), corrected snow (new code 7), and Corrected Land (new code 8).

3.3 SNOTEL and COOP data

SNOTEL sites are automated SNOw TELemetry stations that record real time Snow Water Equivalent (SWE) data as well as snow depth, precipitation and min and max air temperature in their standard configuration. They are spread throughout mountainous areas of the Western US (more than 750 stations) and managed by the Natural Resources Conservation Service. Twenty-one of these stations are in the state of Arizona, but only four fall within the boundary of the study area (see Fig. 1).

In addition, six COOP stations (Cooperative Station Observations, managed by the National Weather Service; NWS 1989) where snow depth is measured exist at lower elevations in the watershed (see Fig. 1), however the available snow depth measurements for WY 2005 are suspicious because they all indicate no snow throughout the winter even though this period indicates high levels of SWE in the SNOTEL data. The COOP station data was therefore not used in this study.

4 Methods applied for cloud removal

Based on the review of previously reported research, we investigated three methods for their effectiveness in cloud removal from MODIS imagery over our study area:

HESSD
9, 13693–13728, 2012

1. combining Terra (MOD10A1) and Aqua (MYD10A1) imagery SCA products,
2. time interpolation,
3. nearest neighbor spatial interpolation informed by elevation and aspect.

In addition we developed and tested a fourth method:

4. probability of snow estimation, via logistic regression informed by elevation and aspect.

Each of these methods was first tested separately to assess the effectiveness of its performance. Subsequently, we implemented and tested a hybrid approach based on sequential application of the afore-mentioned methods.

4.1 Terra/Aqua combination

Combination of MOD10A1 and MYD10A1 SCA images takes advantage of the short (3 h) time interval between the two observations and the transience of clouds during that time. The principal assumption is that snow conditions remain essentially constant (no snow falls or ablates) during that period. If a pixel on the one image is classified as cloud (or error) but is reliably classified as land or snow cover on the other, then the problem pixel is reclassified appropriately. This method was adopted based on the experience of Parajka and Blösch (2008). The algorithm took approximately 12 min to execute on an Intel Pentium-D 2.80 GHz computer.

4.2 Time interpolation

The time-interpolation method employs three temporal windows applied sequentially. The first window removes cloud coverage from image[day] based on snow cover information from image[day−1] and image[day+1]. If a cloudy pixel on image[day] has snow (land) cover on both image[day−1] and image[day+1], then it is reclassified as snow (land) covered. The second window applies a similar logic using image[day−1]

HESSD
9, 13693–13728, 2012

and image[t+2]. Finally, the third window applies a similar logic using image(day−2) and image(day+1). This approach makes the assumption that snow cover remains essentially constant during the spans of the different temporal windows. This assumption may be considered reasonable because the probability of snowmelt tends to be lower during cloudy days. This method was adopted based on the experience of Gafurov and Bárdossy (2009) who modified the temporal windowing approach applied by Parajka and Blösch (2008). The algorithm took approximately 3.2 min to execute on an Intel Pentium D 2.80 GHz computer.

4.3 Nearest neighbor spatial interpolation

The nearest neighbor spatial interpolation method uses information from the eight pixels surrounding (edge and diagonal) a cloudy pixel. If any neighbor pixel has snow cover, is at a *lower elevation*, and has the same aspect, then the cloudy pixel is classified as snow. Once the entire image has been processed, a similar logic is applied to any remaining cloudy pixels – if any neighbor pixel is land covered, at a *higher elevation*, and has the same aspect, the cloudy pixel is classified as land.

A 30 m resolution Digital Elevation Model (DEM) of the area was obtained from the United States Geological Survey (USGS) and processed using the aspect tool of the spatial analyst extension in ArcGIS 9.3. Each pixel was assigned an aspect value from 0° (due north) to 360° (again due north) measured counterclockwise, or a value of −1 if the slope is flat. The aspect of a pixel is the exposure of the terrain represented by that pixel, in other words, the direction in which the slope of the terrain faces (e.g. north, south, northeast, etc.) when it is not flat. The pixels were classified accordingly as north, south, east, west, northeast, southeast, northwest or southwest facing. A re-sampling routine was then run to upscale the "elevation" and "aspect" to the 463.32 m resolution of the SCA images to allow comparison between the three layers of information. The resampling rules "bilinear interpolation" and "majority of pixels" were applied respectively taking into consideration the nature of the data. An elevation raster is a continuous surface and therefore it is most appropriately resampled using a bilinear

HESSD
9, 13693–13728, 2012

interpolation, where the elevation values of the four nearest 30 m input cell centers (used to create the new 463.32 m cell) are averaged. This average is weighted, taking into consideration the proximity of the four nearest 30 m input cell centers to the new 463.32 m cell center. For the aspect raster, the "majority of pixels" rule was used. This rule determines the value of the new cell by choosing the most frequent values of the 30 m input cell centers that are within the new 463.32 m cell.

This method was modified from Gafurov and Bárdossy (2009), who used only elevation information. We included aspect information because topographic controls like elevation, aspect and slope (not used here) can significantly influence energy exchange and melt across a watershed by modifying the exchange of direct-beam and diffuse shortwave radiation and longwave radiation (Dewalle and Rango, 2008). The algorithm took approximately 8 h to execute when run by itself on an Intel Pentium D 2.80 GHz computer.

4.4 Locally weighted logistic regression

The locally weighted logistic regression (LWLR) method uses relationships between the spatial attributes of pixels surrounding a cloudy pixel to estimate the "Probability of Snow Occurrence" (PSO). This method is adapted from Clark and Slater (2006), who used precipitation observations at sparsely located meteorological stations, and spatial maps of elevation, latitude and longitude, to estimate daily precipitation totals across complex terrain in Western Colorado. Here, we used elevation and aspect as the explanatory variables.

To estimate the PSO at a cloudy pixel, the LWLR method weights the information from neighboring pixels inversely with distance, and fits the data to a logistic curve.

HESSD
9, 13693–13728, 2012

The following equations are used to calculate the PSO of a cloudy pixel (PSO_{icloud}):

$$PSO_{icloud} = \frac{1}{1 + \exp\left(-\hat{\boldsymbol{Z}}_{icloud}\hat{\boldsymbol{\beta}}\right)} \quad (1)$$

$$\hat{\boldsymbol{\beta}}_{new} = \hat{\boldsymbol{\beta}}_{old} + \left(\hat{\boldsymbol{X}}^T\hat{\mathbf{W}}\hat{\mathbf{V}}\hat{\mathbf{X}}\right)^{-1}\hat{\boldsymbol{X}}^T\hat{\mathbf{W}}\left(\hat{\boldsymbol{Y}}' - \pi\right) \quad (2)$$

$$\pi = \frac{1}{1 + \exp\left(-\hat{\boldsymbol{X}}_{ipix}\hat{\boldsymbol{\beta}}_{old}\right)} \quad (3)$$

$$\hat{\mathbf{W}} = \mathrm{diag}\left(\hat{\mathbf{w}}_{ipix,ipix} = \left[1 - \left(\frac{d_{ipix}}{MAXD}\right)^3\right]^3\right) \quad (4)$$

$$\hat{\mathbf{V}} = \mathrm{diag}\left(\hat{\mathbf{v}}_{ipix,ipix} = \pi_{ipix}\left[1 - \pi_{ipix}\right]^T\right) \quad (5)$$

where $\boldsymbol{Z}_{icloud}$ is a vector of elevation and aspect information for the cloudy pixels indexed as icloud, $\boldsymbol{X}$ is vector of elevation and aspect information for the non-cloudy pixels, $\boldsymbol{\beta}$ is a vector of parameters, $\boldsymbol{Y}'$ is a 0–1 vector indicating snow occurrence or not on the non-cloudy pixels, $\mathbf{W}$ is a diagonal matrix of weights to be assigned to each non-cloudy pixel, $\mathbf{V}$ is a diagonal matrix of the variance associated with the estimate of snow occurrence at each non-cloudy pixel, π_{ipix} indicates the PSO at each non-cloudy pixel, d_{ipix} is the distance from a non-cloudy pixel to the cloudy pixel, and MAXD is a coefficient specifying the window size used around the cloudy pixel (see Clark and Slater (2006) and Loader (1999) for details regarding implementation).

For this study, we tested different values for MAXD (from 5 to 45 pixels) for their ability to provide statistically robust results, reduce significant numbers of cloudy pixels, and require reasonable computational time. Reliability was evaluated using the Brier Score (BS) verification statistic (see Wilks, 2005) and Clark and Slater (2006) computed from the joint distribution of the LWLR forecast probabilities and the observed snow/land

HESSD
9, 13693–13728, 2012

pixels in the image. Although the best results (not shown) were obtained using MAXD = 45, we instead chose MAXD = 30 due to the relatively high performance achieved using only 1/3 rd of the computer time (22 h as opposed to 67 h on a 2.66 GHz Dual-Core Intel Zeron computer).

Note that LWLR does not, by itself, automatically reclassify cloudy pixels, but only provides an estimate of the probability that the pixel is actually snow or land. Therefore a minimum probability threshold must be selected to convert the probability to a binary outcome. To select this threshold, we conducted a sensitivity analysis by varying the threshold from 0 to 1 in steps of 0.025, and chose the threshold value that minimized the sum of the conditional probabilities of commission and omission errors computed over all non-cloudy pixels inside the window (for details see Lopez-Burgos, 2010). The threshold was separately selected for each cloudy pixel to which LWLR was applied. Figure 4 shows an example of the transition from original to corrected MOD10A1 image (26 November 2004), along with maps of the estimated PSO and the values of the thresholds selected.

5 Results for each cloud removal method applied independently and in sequence

Each of the four methods was first tested separately to assess the effectiveness of its performance. Subsequently, a sequential approach was tested, in which the methods were applied in sequence. Two summary statistics are used to indicate the change achieved by implementation of each method:

$$\%\text{Change} = \left(\frac{\#\text{Corrected}(x_i,t) - \#\text{Original}(x_i,t)}{\#\text{Original}(x_i,t)}\right)\cdot 100 \quad (6)$$

$$\%\text{Cover} = \left(\frac{\#\text{Pixels}(x_i,t)}{\sum_{i=1}^{6}\text{Pixels}(x_i,t)}\right)\cdot 100 \quad (7)$$

HESSD
9, 13693–13728, 2012

where x_i represents codes 1 through 6, and t represents the time period for which the statistic was calculated (e.g. year or month).

We first discuss the results of applying each method separately. The change in % *cover* achieved over the entire study time period by each method is shown in Table 1 for each category. Note that ~ 39 % of the image pixels were initially classified as cloudy. In brief:

1. The Terra/Aqua combination method reduced cloud cover, error and no-decision pixels by ~ 22 %, ~ 97 % and ~ 3.7 % respectively, for an ~ 22.81 % reduction of "bad" pixels. Further, the two days missing in the Terra images time series were not missing in the Aqua images and so a more complete time series was achieved.

2. The time interpolation method reduced cloud cover, error and no-decision pixels by ~ 43 %, ~ 95 % and ~ 46 % respectively, thereby removing more bad pixels than either the Terra/Aqua combination or spatial interpolation methods. However, unlike the Terra/Aqua combination, this method does not give information on missing days.

3. The Nearest Neighbor spatial interpolation method is the least effective of the four methods. Cloud cover, error, and no decision pixels were reduced by only ~ 5 %, 9 % and 0.03 % respectively. Again, this method does not give information on missing days.

4. The Locally Weighted Logistic Regression (LWLR) method achieved the highest effectiveness at reducing cloud cover and no decision pixels (~ 62 % and 60 % respectively), but was significantly less effective than either Terra/Aqua combination or time interpolation at reducing the number of "error" pixels.

Figure 5a shows how the percentage of pixels classified as cloudy in the original MODIS SCA images varies for each month during the study period, from a low of ~ 24 % in April to a high of ~ 69 % in February. Figure 5b–d shows the %change in

HESSD
9, 13693–13728, 2012

clouds, snow and land achieved by each method for each month. Nearest neighbor spatial interpolation is consistently poor at cloud removal, while logistic regression is the most effective. For removing no decision pixels, the Terra/Aqua and time interpolation algorithms perform best. All methods increased amount of snow cover more than they increased amount of land, a reasonable result since the areas with the most consistent cloud cover throughout the study period are the areas of snow accumulation, mainly at higher elevations.

The results above indicate that each method has different strengths and weaknesses. To synergistically exploit the strengths of all four methods, we next applied the methods in sequence (in the order Terra/Aqua combination, time interpolation, spatial interpolation, and locally weighted logistic regression), at each step retaining the results from the previous one. Table 1 shows that the sequential approach achieved a very high degree of cloud cover, error and no-decision pixel removal ($\sim 94\,\%$, $\sim 99\,\%$ and $\sim 64\,\%$ respectively), while increasing the number of snow and land pixels by $\sim 154\,\%$ and $\sim 54\,\%$ respectively – a considerable increase in the amount of SCA indicated by the images. Figure 6 shows the progressive improvement obtained by sequential application of the methods and how this improvement distributes across months. Figure 7 shows the significant change obtained by the sequential method, for the MODIS SCA image of 18 February 2005. The changes achieved by the hybrid approach are clearly substantial, and in marked contrast to the changes achieved by each method applied independently.

6 Evaluation of accuracy of the results

Finally, we assess the accuracy of the results by comparing the SCA images with data from four available SNOTEL sites located in the mountainous zones of the Salt River Basin (Fig. 1). Although the SNOTEL sites are effectively point-scale measurements, their pixel locations were localized using ArcGIS 9.3 by converting the station's point shapefile to a raster with the same extent, resolution and projection of the images. This

HESSD
9, 13693–13728, 2012

raster was then converted to an ASCII file for processing. Several evaluation statistics were calculated for (a) the original MOD10A1 and MYD10A1 images, (b) each cloud removal method applied separately, and (c) the sequential cloud removal approach. For each SNOTEL site pixel, the hit, false alarm, miss and correct rejection rates were computed for each day of the available time series.

A simple approach to evaluation would be to consider each SNOTEL site pixel to be snow covered if the corresponding SNOTEL station has recorded measurable SWE (SWE > 0). This assumption would imply that each station measurement, corresponding to an area of approximately 9 m^2 (snow pillow standard size is 3 × 3 m), is representative of conditions across the entire 500 × 500 m (250 km^2) image pixel. However, this assumption can be poor for several reasons, an important one being that the MODIS sensor fails to map snow when snow depths are less than 4 cm (Hall and Riggs, 2007). Based on an average snow density of 0.3621 $g\,cm^{-3}$ (average snow density for one of our SNOTEL stations during WY 2005), 4cm of depth corresponds to approximately 0.57 inches of SWE. Therefore, to establish a more accurate basis for evaluation, a sensitivity analysis was performed to find a threshold value of recorded SWE above which the pixel could be considered to be snow covered. To do this, the SNOTEL station raster was used as the observed ground truth and the MODIS SCA images as the modeled forecast. The conditional probabilities of hits (observed = snow/forecast = snow), false alarms (observed = no snow/forecast = snow), misses (observed = snow, forecast = no snow) and correct rejections (observed = no snow/forecast = no snow) were computed for 20 different threshold SWE values (from 0 to the maximum value of SWE = 19.5 inches recorded at the stations over the observation time period), and an optimal threshold (SWE = 1.0263 inches) was selected that minimized the sum of the conditional probabilities of misses and false alarms while maximizing the sum of the conditional probabilities of hits and correct rejections.

HESSD
9, 13693–13728, 2012

The following evaluation statistics recommended by Wilks (1995) were then computed:

$$\mathrm{PC} = \frac{a+d}{n} \tag{8}$$

$$\mathrm{TS} = \frac{a}{a+b+c} \tag{9}$$

$$B = \frac{a+b}{a+c} \tag{10}$$

$$\mathrm{FAR} = \frac{b}{a+b} \tag{11}$$

$$H = \frac{a}{a+c} \tag{12}$$

where a = number of hits, b = number of false alarms, c = number of misses, d = number of correct rejections, and $n = a+b+c+d$. The Proportion Correct (PC) and Threat Score (TS) are accuracy statistics, while B is a measure of bias, the False Alarm Ration (FAR) is a measure of reliability and the Hit rate (H) is a measure of discrimination.

The Proportion Correct is a good measure of accuracy if the event (snow) and non-event (no snow) occurred with equal frequency (i.e. 50/50). A completely accurate estimator will achieve a PC = 1 ($b = c = 0$) while a completely inaccurate estimator will have a PC = 0 ($a = d = 0$). However, since snow cover in the Salt River Basin is less frequent than no-snow cover, the Threat Score is a better accuracy statistic; an accurate estimator will achieve a TS = 1 ($b = c = 0$) while an inaccurate estimator will have a TS = 0 ($a = 0$). An unbiased estimator will achieve $B = 1$ ($b = c = 0$); $B > 1$ indicates that snow is estimated more often than observed, while $B < 1$ indicates that snow is estimated less often than observed. A good estimator will also achieve a False Alarm Ratio close to 0 (no false alarms) while FAR close to 1 indicates very poor performance (no hits). Finally, a good estimator will achieve a Hit Rate close to 1 (no misses).

The results are summarized in Table 2. We see that:

HESSD
9, 13693–13728, 2012

1. the time interpolation method achieves the best overall accuracy, and provides consistently better evaluation statistics – better even than those of the original images. This is likely due to the larger number of cloud free pixels, and therefore a higher amount of estimate-observation pairs used in computing the statistics.

2. The other three methods have varying results, with LWLR achieving the worst PC, TS, *B* and *H* statistics.

3. The sequential approach is second best in terms of accuracy (PC = 84 %, TS = 74 %), matches time interpolation in terms of bias (10 %), is middling in terms of false alarms (10 %) and second in terms of hit rate (*H* = 81 %).

7 Discussion and conclusions

7.1 Differences in performance between the cloud removal algorithms

The cloud removal algorithms examined in this study gave differing results with regards to the number of cloudy pixels removed. In terms of number of cloudy pixels removed, LWLR was best, followed by time interpolation, and Terra/Aqua combination in that order. Spatial interpolation provided very little cloud removal performance. When removing clouds, all methods added more snow pixels than land pixels, a reasonable result since clouds tend to concentrate at higher elevations where more snow accumulates. Overall, the sequential approach achieved a 94 % reduction in cloud cover (from 38.7683 % to 2.4084 %), which can be considered to be very successful. The results would, of course, be even better if we did not include images from days that were completely covered by clouds and for which the algorithms had little effect.

It is likely that LWLR is able to remove more cloudy pixels than any other method because it uses information from a window of pixels of area $\sim 775\,\mathrm{km}^2$ around each cloudy pixel (~ 7 % of the total area of the watershed). This gives the method an advantage over the other algorithms, which only draw upon information at the same pixel

HESSD
9, 13693–13728, 2012

or in the 8 pixels neighborhood having an area of 0.86 km^2. Because the Terra/Aqua combination and Time Interpolation methods depend on the dispersion of clouds during the time step, cloud cover that persists for several days can confound the methods. In contrast, even if clouds persist at higher elevations for several days in a row, the LWLR method can use information from non-cloudy pixels at lower elevations.

On the other hand, LWLR is unable to remove cloud cover on days when clouds cover all or much of the watershed. In such situations, the Terra/Aqua combination and time interpolation methods can be effective, provided the clouds do not persist for too many days. Further, the Terra/Aqua combination helps to complete the time series, a positive and useful aspect that none of the other algorithms possess.

Taken together, it therefore makes logical sense that a sequential combination of these three algorithms (LWLR, Terra/Aqua combination and Time Interpolation) should provide synergistic effects. Overall, spatial interpolation provides only minor improvements, and its abilities are partially replicated by the LWLR approach. Elimination of this method from the sequence will reduce processing time and have very little overall impact on the results.

7.2 Differences in evaluation results between the cloud removal algorithms

time interpolation provides the best overall accuracy with consistently better evaluation statistics (better than that of the original images). LWLR removes the largest amount of cloud cover but has worse evaluation performance, due inherently to the extrapolation of information from surrounding pixels. This may be aggravated by the large window size used.

Terra/Aqua combination also reduces accuracy even though the observations are from the same day and the instruments should give similar results. One reason for this may be that the MODIS instrument aboard Aqua has degraded data quality in band 6 (70 % of the band 6 detectors have been identified as non-functional), pertaining to the short-wave infrared portion of the electromagnetic spectrum (~ 1.6 µm) where snow

HESSD
9, 13693–13728, 2012

surfaces have low reflectance, and used in the computation of Normal Difference Snow Index (NDSI) used for SCA computations. As a consequence, band 6 was substituted with band 7 in an Aqua-specific algorithm to map snow. The 2007 accuracy of the Aqua MYD10A1 images had not yet been assessed (Hall and Riggs, 2007) and no papers were found that do so.

Overall, sequential application of the methods achieved accuracy similar to that of original MOD10A1 image, with improvements in certain areas. Further, the Threat Score increased (which means that more pixels were correctly classified as snow), the Bias came closer to one (meaning that in general there were relatively more hits than misses and false alarms and under-estimation of snow events was reduced), and the Hit Rate moved closer to one (meaning that more pixels were correctly classified as snow).

7.3 Conclusions

The sequential cloud removal approach has the potential to be applied successfully at other locations. Whereas the Terra/Aqua combination, Time Interpolation and spatial interpolation methods have been previously tested in watersheds having different topographical and climate characteristics (Parajka and Blösch, 2008; Gafurov and Bárdossy, 2009), the LWLR Probability of snow method has not previously been used for cloud removal and SCA estimation. It should therefore be subjected to more extensive testing. It may also be interesting to examine whether the additional use of slope information as an explanatory variables would prove helpful.

Our future work will include the assimilation of corrected SCA images into a distributed hydrologic model to reduce the uncertainty of streamflow forecasts. Mcguire et al. (2005) and Andreadis and Lettenmaier (2006) have demonstrated that although assimilation of MOD10A1 images into the variable infiltration capacity model can provide favorable results, cloud cover reduces the usefulness of this data and requires the data to be assimilated in a non-continuous manner. Since removal of cloud cover can result in considerably larger estimates of snow, as seen on Sect. 5 of this paper,

HESSD
9, 13693–13728, 2012

application of the algorithm developed in this work should help to simplify the assimilation process while improving the model estimates of various hydrological states and fluxes.

Acknowledgement. This work was supported in part by (1) the NASA Applied Earth Sciences Program through Cooperative Agreement (NNAO6CN09A) funding to the WaterNET project (The NASA Water Cycle Solutions Network), (2) the NSF Science and Technology Center for Sustainability of semi-Arid Hydrology and Riparian Areas (SAHRA), (3) the Department of Hydrology and Water Resources at the University of Arizona, (4) the Salt River Project (SRP), (5) the US Bureau of Reclamation, and (6) the US Army Corps of Engineers. The first author was supported by an NSF "Graduate Education for Minorities (GEM)" Fellowship. Assistance, ideas and technical support by Guillermo Martínez-Baquero, Seshadri Rajagopal and Matej Durcik are gratefully acknowledged.

References

Ackerman, S. A., Strabala, K. I., Menzel, P. W. P., Frey, R. A., Moeller, C. C., and Gumley, L. E.: Discriminating clear sky from clouds with MODIS, J. Geophys Res., 103, 32141–32157, 1998.

Andreadis, K. M. and Lettenmaier, D. P.: Assimilating remotely sensed snow observations into a macroscale hydrology model, Adv. Water Resour., 29, 872–886, 2006.

Bitner, D., Carroll, T., Cline, D., and Romanov, P.: An assessment of the differences between three satellite snow cover mapping techniques, Hydrol. Process., 16, 3723–3733, 2002.

Carroll T., Cline, D., Fall, G., Nilsson, A., Li, L., and Rost, A.: NOHRSC operations and the simulation of snow cover properties for the conterminous US, 69 Annual Meeting of the Western Snow Conference, Sun Valley, Idaho, 16–19 April 2001, available at: http://www.westernsnowconference.org/proceedings/2001.htm, 2001.

Caves, R., Turpin, O., Clark, C., Ferguson, R., and Quegan, S.: Comparison of SCA derived from different satellites sensors: implications for hydrological modeling, in: RSS 99: Earth Observations: From Data to Information: Proceedings of the 25th Annual Conference and Exhibition of the Remote Sensing Society, Cardiff, Wales, 8–10 September 1999, 545–552, 1999.

HESSD

9, 13693–13728, 2012

Cayan, D. R.: Interannual climate variability and snowpack in the Western United States, J. Climate, 9, 928–948, 1996.
Clark, M. P. and Slater, A. G.: Probabilistic quantitative precipitation estimation in complex terrain, J. Hydrometeorol., 7, 3–22, 2006.
Dewalle, D. R. and Rango, A.: Principles of Snow Hydrology 1st Edn., Cambridge University Press, 420 pp., 2008.
Earman, S., Campbell, A. R., Phillips, F. M., and Newman, B. D.: Isotopic exchange between snow and atmospheric water vapor: estimation of the snowmelt component of groundwater recharge in the Southwestern United States, J. Geophys. Res., 111, D09302, doi:10.1029/2005JD006470, 2006.
Fassnacht, S. R., Dressler, K. A., and Bales, R. C.: Snow water equivalent interpolation for the Colorado River basin from snow telemetry (SNOTEL) data, Water Resour. Res., 39, 1208, doi:10.1029/2002WR001512, 2003.
Gafurov, A. and Bárdossy, A.: Cloud removal methodology from MODIS snow cover product, Hydrol. Earth Syst. Sci., 13, 1361–1373, doi:10.5194/hess-13-1361-2009, 2009.
Gedalof, Z. and Smith, D. J.: Interdecadal climate variability and régime-scale shifts in Pacific North America, Geophys. Res. Lett., 28, 1515–1518, 2001.
Hall, D. K. and Riggs, G. A.: Accuracy assessment of the MODIS snow products, Hydrol. Process., 21, 1534–1547, 2007.
Hawkins, T. W.: Parameterization of the snowmelt runoff model for the Salt-Verde System, Arizona during drought conditions, Journal of the Arizona-Nevada Academy of Science, 38, 66–73, 2006.
Hereford, R., Webb, R. H., and Graham, S.: Precipitation History of the Colorado Plateau Region, 1900–2000, USGS Fact Sheet 119-02, available at: http://pubs.usgs.gov/fs/2002/fs119-02/fs119-02.pdf (last access: 3 December 2012), 2002.
Hirschboeck, K. K. and Meko, D. M.: A Tree-Ring Based Assessment of Synchronous Extreme Streamflow Episodes in the Upper Colorado and Salt-Verde-Tonto River Basins Final Report: a collaborative Project between The University of Arizona's Laboratory of Tree-Ring Research and The Salt River Project, available at: Phttp://fp.arizona.edu/kkh/SRP/Final.Report/Final.Final.Report.pdf (last access: 3 December 2012), 2005.
Jacobs, K. L., Garfin, G. M., and Morehouse, B. J.: Climate science and drought planning: the Arizona experience, J. Am. Water Resour. As., 41, 437–445, 2005.

HESSD
9, 13693–13728, 2012

Justice, C. O., Vermote, E., Townshend, J. R. G., Defries, R., Roy, D. P., Hall, D. K., Salomonson, V. V., Privette, J. L., Riggs, G., Strahler A., Lucht, W., Myneni, R. B., Knyazikhin, Y., Running, S. W., Nemani, R. R., Wan, Z. M., Huete, A. R., van Leeuwen, W., Wolfe, R. E, Giglio, L., Muller, J. P., Lewis, P., and Barnsley, M. J.: The moderate resolution imaging spectroradiometer (MODIS): land remote sensing for global change research, IEEE T. Geosci. Remote, 36, 1228–1249, 1998.

Klein, A. G. and Barnett, A. C.: Validation of daily MODIS snow cover maps of the Upper Rio Grande River Basin for the 2000–2001 snow year, Remote Sens. Environ., 86, 162–176, 2003.

Klein, A. G., Hall, D. K., and Riggs, G. A.: Improving snow-cover mapping in forests through the use of a canopy reflectance model, Hydrol. Process., 12, 1723–1744, 1998.

Klein, A. G., Hall, D. K., and Nolin, A. W.: Development of a prototype snow albedo algorithm for the NASA MODIS instrument, in: Proceedings of the 57th Eastern Snow Conference, 15–17 May 2000, Syracuse, NY, 143–157, 2000.

Lichtenegger, J., Seidel, K., Keller, M., and Haefner, H.: Snow surface measurements from digital Landsat MSS data, Nord. Hydrol., 12, 275–288, 1981.

Loader, C: Local Regression and Likelihood, Springer, New York, New York, 308 pp., 1999.

López-Burgos, V.: Reducing Cloud Obscuration on MODIS Snow Cover Area Products by Applying Spatio-Temporal Techniques Combined with Topographic Effects, MS Thesis, Department of Hydrology and Water Resources, The University of Arizona, Tucson, AZ, 124 pp., 2010.

Lucas, R. M. and Harrison, A. R.: Snow observation by satellite: a review, Remote Sens. Rev., 4, 285–348, 1990.

McGuire, M., Wood, A. W., Hamlet, A. F., and Lettenmaier, D. P.: Use of satellite data for streamflow and reservoir storage forecasts in the Snake River Basin, ID, J Water Res. Pl.-Asce, 132, 97–110, doi:10.1061/(ASCE)0733-9496(2006)132:2(97), 2005.

Maurer, E. P., Rhoads, J. D., Dubayah, R. O., and Lettenmaier, D. P.: Evaluation of the snow-covered area data product from MODIS, Hydrol. Process., 17, 59–71, 2003.

Megdal, S: Securing Sustainable Water Supplies in Arizona, IDS-Water-White Paper, available at: http://www.idswater.com/Common/Paper/Paper_143/Securing%20Sustainable%20Water%20Supplies%20in%20Arizona.htm (last access: 3 December 2012), 2004.

HESSD
9, 13693–13728, 2012

Molotch, N. P., Fassnacht, S. R., Bales, R. C., and Helfrich, S. R.: Estimating the distribution of snow water equivalent and snow extent beneath cloud cover in the Salt-Verde River basin, Arizona, Hydrol. Process., 18, 1595–1611, 2004.
National Weather Service: National Weather Service Observing Handbook No. 2: Cooperative Station Observations, Silver Spring, Maryland, 1989.
Ostler, D. A.: Upper Colorado River Basin perspectives on the drought, Southwest Hydrology: The Resource for Semi-Arid Hydrology, 4, p. 18 and p. 29, 2005.
Parajka, J. and Blöschl, G.: Validation of MODIS snow cover images over Austria, Hydrol. Earth Syst. Sci., 10, 679–689, doi:10.5194/hess-10-679-2006, 2006.
Parajka, J. and Blösch, G.: Spatio-temporal combination of MODIS images – potential for snow cover mapping, Water Resour. Res., 44, W03406, doi:10.1029/2007WR006204, 2008.
Piechota, T., Timisena, J., Tootle, G., and Hidalgo, H.: The Western US drought: how bad is it?, Eos, 85, 301–304, 2004.
PRISM Climate Group at Oregon State University: United States Average Monthly or Annual Maximum Temperature, 1971-2000, available at: http://www.prism.oregonstate.edu/products/matrix.phtml?vartype=tmax&view=data (last access: 3 December 2012), 2006a.
PRISM Climate Group at Oregon State University: United States Average Monthly or Annual Minimum Temperature, 1971-2000, available at: http://www.prism.oregonstate.edu/products/matrix.phtml?vartype=tmin&view=data (last access: 3 December 2012), 2006b.
Rango, A.: The snowmelt-runoff model, in: Proceedings of the ARS Natural Resources Modeling Symposium, Pinyree Park, CO, 16–21 October 1983, 321–325, 1985.
Rinne, J. N.: Hydrology of the Salt River and its reservoirs, Central Arizona, Journal of the Arizona Academy of Science, 10, 75–86, 1975.
Rodell, M. and Houser, P. R.: Updating a land surface model with MODIS-derived snow cover, J. Hydrometeorol., 5, 1064–1075, 2004.
Schmugge, T. J., Kustas, W. P., Ritchie, J. C., Jackson, T. J., and Rango, A.: Remote sensing in hydrology, Adv. Water Resour., 25, 1367–1385, 2002.
Seidel, K., Ade, F., and Lichtenegger, J.: Aumenting LANDSAT MASS data with topographic information for enhanced registration and classification, IEEE T. Geosci. Remote, GE-21, 252–258, 1983.
Serreze, M. C., Clark, M. P., Armstrong, R. L., McGuiness, D. A., and Pulwarty, R. S.: Characteristics of the Western United States snowpack from snowpack telemetry (SNOTEL) data, Water Resour. Res., 35, 2145–2160, 1999.

HESSD
9, 13693–13728, 2012

Sheppard, P. R., Comrie, A. C., Packin, G. D., Angersbach, K., and Hughes, M. K.: The climate of the US Southwest, Clim. Res., 21, 219–238, 2002.
Simic, A., Fernandes, R., Brown, R., Romanov, P., and Park, W.: Validation of Vegetation, MODIS, and GOES+SSM/I snow cover products over Canada based on surface snow depth observations, Hydrol. Process., 18, 1089–1104, 2004.
Tekeli, A., Akyürek, Z., Sorman, A. A., Sensoy, A., and Sorman, A. Ü.: Using MODIS snow cover maps in modeling snowmelt runoff process in the eastern part of Turkey, Remote Sens. Environ., 97, 216–230, 2005.
Wilks, D. S.: Statistical Methods in the Atmospheric Sciences 2nd Edn., Academic Press, Burlington, Massachusetts, 648 pp., 2005.
Wolfe, R. E., Roy, D. P., and Vermonte, E.: MODIS land data storage, gridding, and compositing methodology: level 2 grid, IEEE T. Geosci. Remote, 36, 1324–1338, 1998.
Zhou, X., Xie, H., and Hendrickx, J. M. H.: Statistical evaluation of remotely sensed snow-cover products with constraints from streamflow and SNOTEL measurements, Remote Sens. Environ., 94, 214–231, 2005.

HESSD
9, 13693–13728, 2012

Table 1. Change in total period "%Cover" of the MOD10A1 images, achieved by each method for each category.

Method	Cloud	Error	Snow	Land	No Decision	Missing Day
Initial	38.77	0.064	4.52	55.80	0.025	0.823
T/A Combination	30.00	0.002	6.07	63.93	0.024	0
%Change	−22.71	−96.71	+34.50	+14.57	−3.74	−100
time interpolation	21.95	0.004	6.02	71.18	0.014	0.823
%Change	−43.37	−94.56	+33.33	+27.56	−45.50	0
spatial interpol.	36.94	0.058	4.79	57.36	0.025	0.823
%Change	−4.72	−9.45	+6.13	+2.80	−0.032	0
LWLR (30 pixels)	14.67	0.036	8.86	75.60	0.01	0.823
%Change	−62.16	−44.10	+96.14	+35.48	−60.27	0
Sequential	2.41	0.001	11.47	86.11	0.009	0
%Change	−93.79	−98.90	+153.9	+54.32	−63.79	−100

HESSD
9, 13693–13728, 2012

Table 2. Evaluation statistics for the original images and results.

Method	PC	TS	*B*	FAR	*H*
Unaltered Terra	0.85	0.73	0.85	0.08	0.78
Unaltered Aqua	0.82	0.68	0.91	0.15	0.77
T/A combination	0.83	0.71	0.89	0.12	0.78
Time interpolation	0.88	0.79	0.90	0.07	0.84
Spatial interpol.	0.85	0.73	0.86	0.09	0.78
LWLR	0.80	0.67	0.81	0.10	0.73
Sequential	0.84	0.74	0.90	0.10	0.81

HESSD
9, 13693–13728, 2012

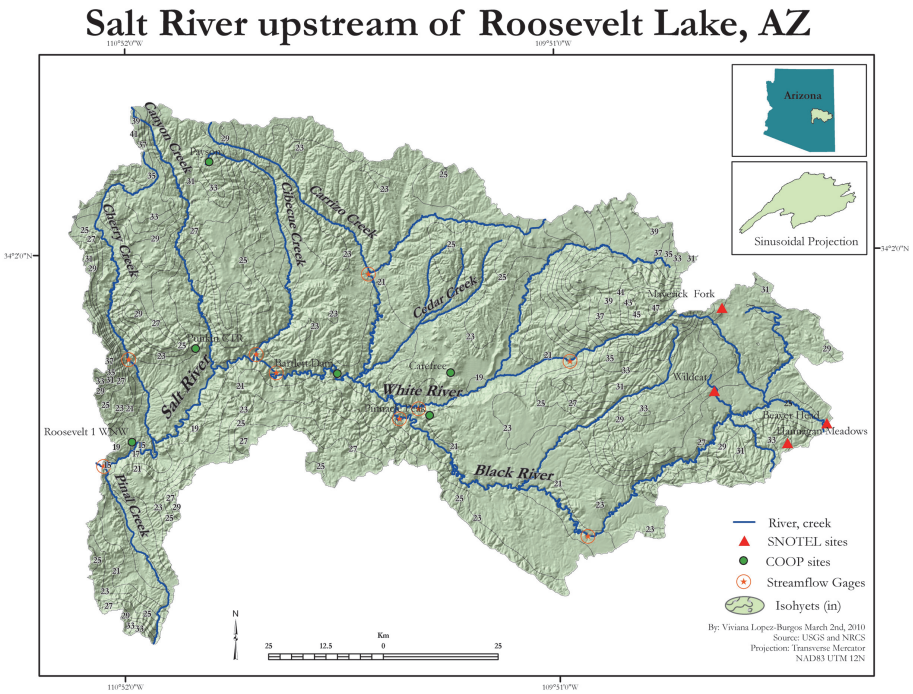

Fig. 1. The Upper Salt River basin.

HESSD
9, 13693–13728, 2012

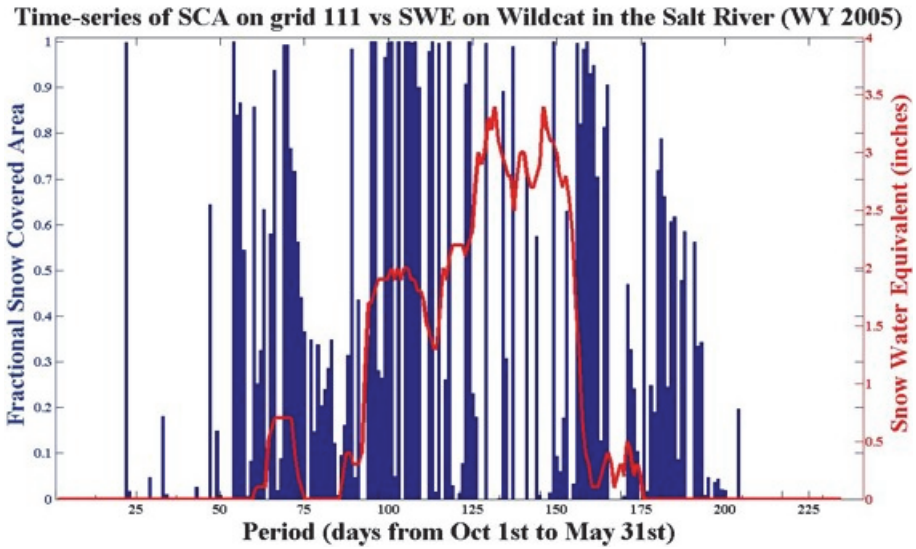

Fig. 2. Fractional Snow Covered Area time series for one grid, overlayed upon a Snow Water Equivalent time series for a SNOTEL station located inside the grid. This plot illustrates the large extent to which clouds cover the watershed during the study period.

HESSD
9, 13693–13728, 2012

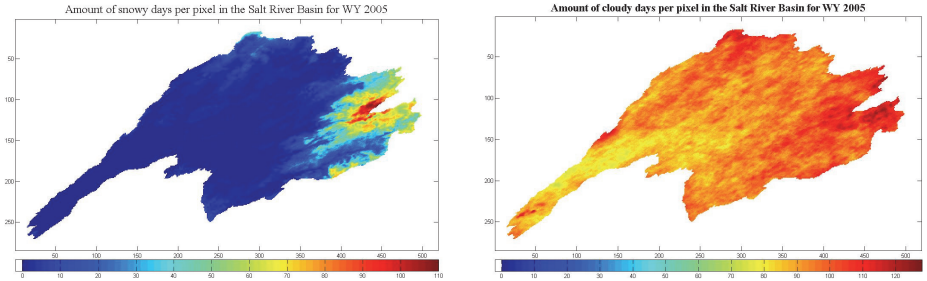

Fig. 3. (a) Pixel map of number of "days of snow" across the basin between 1 October and 31 May, indicating that snow is accumulated at higher elevations on the eastern side; **(b)** pixel map of number of days with clouds over the same period.

HESSD
9, 13693–13728, 2012

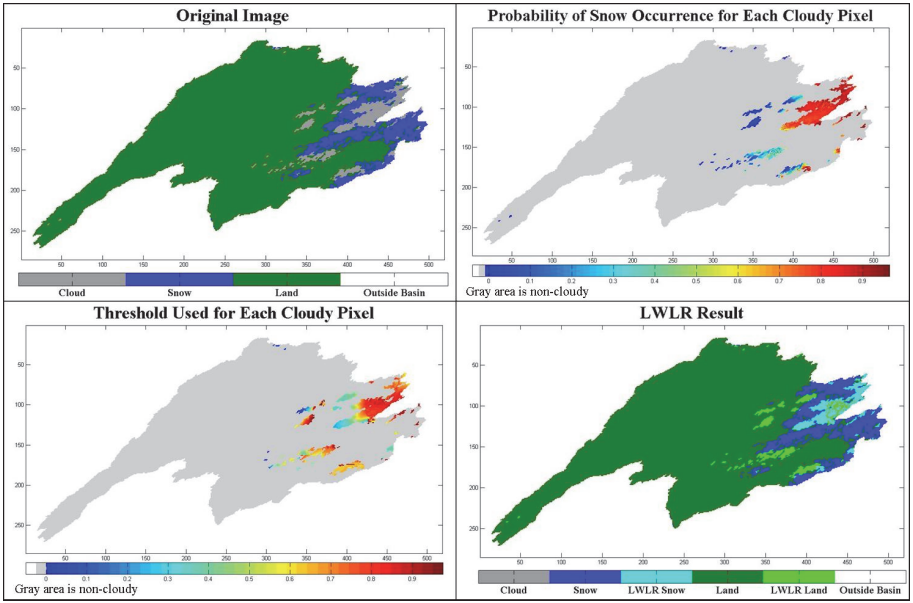

Fig. 4. Example of the transition from original to corrected MOD10A1 image (26 November 2004), along with maps of the estimated PSO and the values of the thresholds selected.

HESSD
9, 13693–13728, 2012

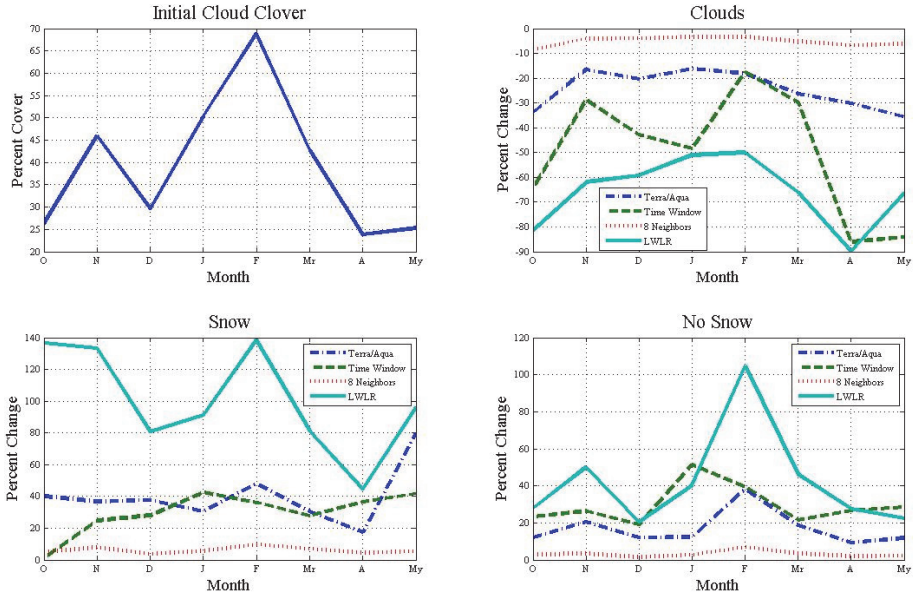

Fig. 5. (a) Shows how the percentage of pixels classified as cloudy in the original MODIS SCA images varies for each month during the study period; subplots **(b)**, **(c)** and **(d)** show the corresponding %Change in clouds, snow and land achieved by each method for each month.

HESSD
9, 13693–13728, 2012

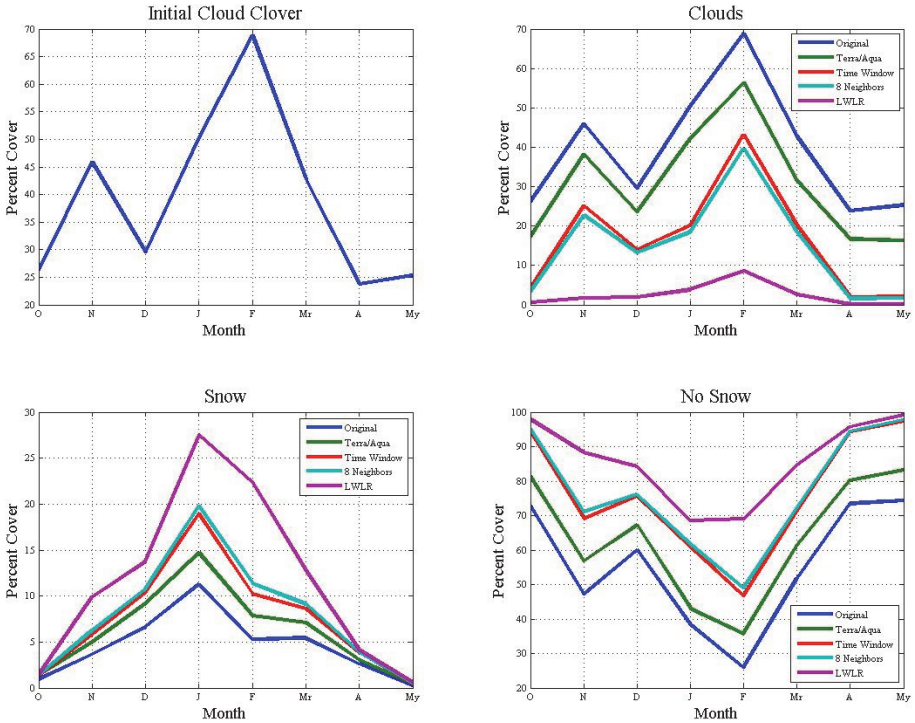

Fig. 6. Progressive improvement obtained by sequential application of the methods and how this improvement distributes across months.

HESSD
9, 13693–13728, 2012

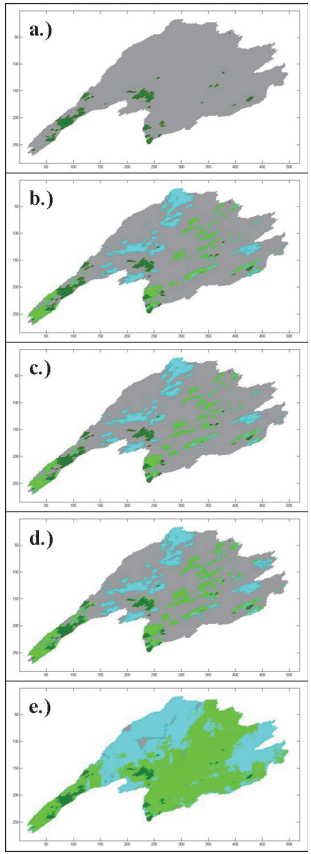

Fig. 7. Example of the sequence results for 18 February 2005; **(a)** original image, **(b)** after T/A combination, **(c)** after time interpolation, **(d)** after spatial interpolation, **(e)** after logistic regression (final result).

HESSD
9, 13693–13728, 2012